How to cite: *Angew. Chem. Int. Ed.* **2024**, *63*, e202314988
doi.org/10.1002/anie.202314988

VIP COFs for Photocatalysis Very Important Paper

Turning on Singlet Oxygen Generation by Outer-Sphere Microenvironment Modulation in Porphyrinic Covalent Organic Frameworks for Photocatalytic Oxidation

Suleman Suleman, Yi Zhang, Yunyang Qian, Jinwei Zhang, Zhongyuan Lin, Önder Metin, Zheng Meng, and Hai-Long Jiang**

Abstract: Singlet oxygen ($^1O_2$) is ubiquitously involved in various photocatalytic oxidation reactions; however, efficient and selective production of $^1O_2$ is still challenging. Herein, we reported the synthesis of nickel porphyrin-based covalent organic frameworks (COFs) incorporating functional groups with different electron-donating/-withdrawing features on their pore walls. These functional groups established a dedicated outer-sphere microenvironment surrounding the Ni catalytic center that tunes the activity of the COFs for $^1O_2$-mediated thioether oxidation. With the increase of the electron-donating ability of functional groups, the modulated outer-sphere microenvironment turns on the catalytic activity from a yield of nearly zero by the cyano group functionalized COF to an excellent yield of 98 % by the methoxy group functionalized one. Electronic property investigation and density-functional theory (DFT) calculations suggested that the distinct excitonic behaviors attributed to the diverse band energy levels and orbital compositions are responsible for the different activities. This study represents the first regulation of generating reactive oxygen species (ROS) based on the strategy of outer-sphere microenvironment modulation in COFs.

Introduction

Light-assisted oxidation reaction represents a sustainable strategy to convert solar energy into highly value-added chemicals.[1] In these reactions, ROS, including singlet oxygen ($^1O_2$), superoxide ($O_2^{\bullet-}$), and hydroxyl radical ($^\bullet$OH), enable the cleavage of chemical bonds and the introduction of oxygen atoms, contributing to efficient conversion of substrates under light irradiation. Due to the unique reactivity and oxidizability of ROS, the investigation of the specific ROS involved in a particular photooxidation reaction has been of considerable interest.[2] Among various ROS, electrically neutral $^1O_2$ is one of the most important ROS with a long lifetime and adequate oxidizability, which has been utilized in various important reactions.[3] The $^1O_2$ can be produced through an energy transfer process from the triplet state (T_1) of a molecular photocatalyst to the ground state of molecular oxygen ($^3O_2$), which relies on the effectiveness of T_1 generation of the photocatalyst. To sensitize the ground-state oxygen into $^1O_2$, a highly effective photocatalyst is necessary.[4] Up to date, the majority of $^1O_2$ is usually produced with the assistance of organic dyes bearing heavy atoms, such as iodine or bromine, transition metal complexes, and noble metal nanoparticles.[5] Although the heavy atoms promote photosensitizers' intersystem crossing (ISC) from singlet to triplet excited states to facilitate the sensitization of $^3O_2$ into $^1O_2$, the application of these conventional photosensitizers in photooxidation reactions is constrained by their lack of selectivity, susceptibility to photobleaching, and toxicity. On the other hand, transition metal complexes and noble metal nanoparticles have raised environmental concerns and have limited availability. Therefore, it is preferable to develop an alternate method to improve $^1O_2$ production.[6]

Recently, metal-nitrogen-doped carbon (MN/C) materials such as Co–N, Cu–N, or Ni–N, have shown great potential for activating molecular oxygen to $^1O_2$. Catalysts with metal ions chelated with nitrogen, which share a similar structure to metal porphyrins or metal phthalocyanines, can efficiently adsorb and activate oxygen,[7] favoring $^1O_2$ photosensitization.[8] In this respect, a few approaches have been developed to manipulate the electronic configurations of catalytic sites of MN/C for improved activity, such as linker engineering, metal node variation, and active guest incorporations.[9] Amongst these strategies, the direct manipulation of the coordination environment around the catalytic metal centers is a particularly effective method for modulating the electronic structures of transition metal complexes. Nevertheless, the majority of strategies employed to modify the coordination environments of transition metal complexes are centered on the primary coordination spheres, in

[*] S. Suleman, Y. Zhang, Dr. Y. Qian, J. Zhang, Z. Lin, Prof. Dr. Z. Meng, Prof. Dr. H.-L. Jiang
Hefei National Research Center for Physical Sciences at the Microscale, Department of Chemistry, University of Science and Technology of China
Hefei, Anhui 230026 (P. R. China)
E-mail: zhengmeng@ustc.edu.cn
jianglab@ustc.edu.cn
Homepage: https://mof.ustc.edu.cn/
Assoc. Prof. Dr. Ö. Metin
Department of Chemistry, College of Sciences, Koç University
Istanbul, 34450 (Türkiye)
Homepage: https://metinresearchgroup.ku.edu.tr/

which the catalytic behavior of the materials is largely constrained by the intrinsic properties of the metal centers.[10] Indeed, the functionalities of active sites are linked to the outer-sphere microenvironment where they exist, thereby significantly altering the catalytic performance of catalysts.[9,11] Increasing evidence indicates that the control of the outer-sphere microenvironment surrounding a catalytic center of enzymes can significantly enhance selectivity and activity by optimizing the substrate binding, stabilizing transition states, and facilitating efficient product release.[12] However, attaining such precise control over the periphery of an active site remains a formidable synthetic challenge, particularly for heterogeneous catalytic systems.[13] Therefore, it is highly desirable to develop photocatalysts with atomically precise and highly customizable structures that allow effective outer-sphere microenvironment modulation.

In this context, COFs represent a distinctive class of crystalline porous materials constructed through the interconnection of organic building blocks via covalent bonds.[14] COFs exhibit large surface area, adjustable pore size, and excellent compositional and structural tailorability, which are desirable prospects for coordination sphere modulation.[15] The compositional flexibility offered by the choice of building blocks and their connections can be regulated to improve stability. More importantly, different functionalities can be feasibly introduced into COFs through various post-modification methods, which would further allow the precise modulation of metal electronic properties based on the unique chemical characteristics of these groups. Despite the features of COFs offer an excellent foundation for overcoming the limitations found in conventional materials for regulating ROS generation in modulating electronic properties,[16] no previous studies have documented the manipulation of ROS generation pathways through the variation of the outer-sphere environment surrounding catalytic metal sites of COFs.

Given the aforementioned points, herein, we report the synthesis of a series of COFs bearing different electron-withdrawing and -donating groups (-R=-CN, -CF_3, -COOMe, -H, and -OMe) on their pore walls, named COF-366(Ni)-R. The -R groups are introduced to COF-366(Ni) through a post-modification based on the Povarov reaction between aryl imines of COF-366(Ni) and different aryl alkynes, which gives isoreticular COF-366(Ni)-R series with distinct functional groups. With the increase of the electron-donating ability of -R groups, COF-366(Ni)-R showed enhanced activity in the photocatalytic oxidation of thioether, in which the yield boosts from nearly zero in the cyano group functionalized COF to up to 98% in the methoxy group functionalized one. Analysis of electronic properties and DFT calculations indicated that the observed different excitonic behaviors are associated with variations in band energy levels and orbital composition. These findings offer valuable insights into generating ROS by modulating the outer-sphere microenvironment of COFs.

Results and Discussion

The COF-366(Ni) was synthesized by the solvothermal method through condensation between 5,10,15,20-tetrakis(4-aminophenyl)porphinato] nickel (Ni-TAP) and 2,5-dimethoxyterephthaldehyde (DMTA) in mixed solvents of 1,2-dichlorobenzene (*o*-DCB) and butanol in the presence of 6 M aqueous acetic acid.[17] Post-synthetic modifications using the Povarov reaction were then performed by reacting COF-366(Ni) with a series of benzene alkynes, which allowed the introduction of different electron-withdrawing and electron-donating functional moieties, including -CN, -CF_3, -COOMe, -H, and -OMe, onto the pore walls of COF-366(Ni) via the formation of quinoline ring to give COF-366(Ni)-R (Figure 1).[18]

The powder X-ray diffraction (PXRD) patterns of COF-366(Ni)-R display peaks at 2θ = 3.43°, 6.89°, and 10.34° (Figure 2a), corresponding to diffractions of (100), (200), and (300), respectively, which are consistent with those of COF-366(Ni), implying that COF-366(Ni)-R are highly crystalline and isostructural with COF-366(Ni). Fourier

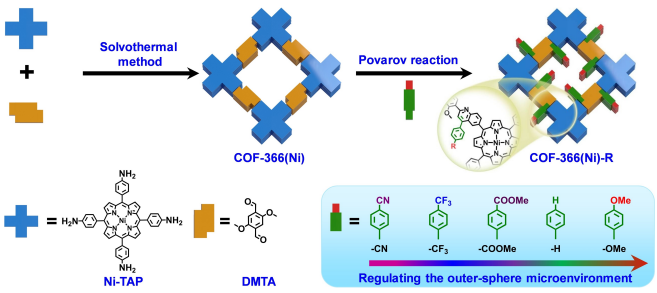

Figure 1. Schematic representation of the outer-sphere microenvironment modulation of Ni sites in COF-366(Ni)-R (-R=-CN, -CF_3, -COOMe, -H, and -OMe).

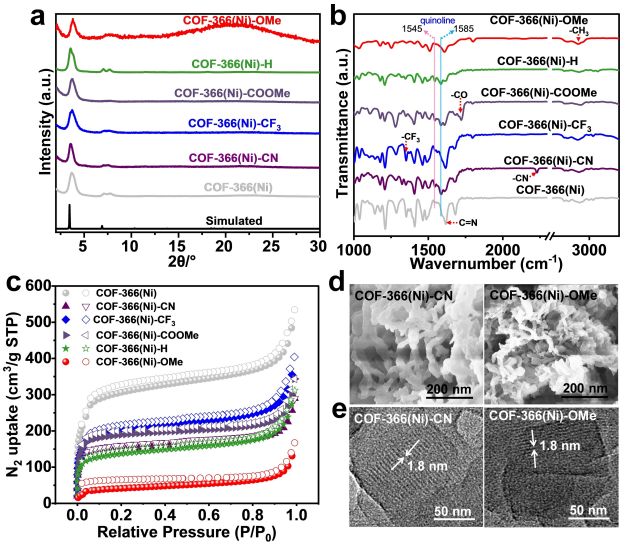

Figure 2. (a) PXRD patterns, (b) FT-IR spectra, and (c) N_2 sorption isotherms at 77 K of COF-366(Ni) and COF-366(Ni)-R. (d) SEM and (e) TEM images for COF-366(Ni)-OMe and COF-366(Ni)-CN.

transform infrared (FT-IR) spectra revealed that the C=N stretching vibrations at 1615 cm^{-1} were retained after the post-synthetic modifications. Moreover, typical stretching vibration peaks at 2931 cm^{-1}, 1208 cm^{-1}, 1721 cm^{-1}, 1347 cm^{-1}, and 2232 cm^{-1} appear, which are respectively ascribed to -CH_3, -H, -CO, -CF_3, and -CN in COF-366(Ni)-OMe, COF-366(Ni)-H, COF-366(Ni)-COOMe, COF-366(Ni)-CF_3, and COF-366(Ni)-CN, unambiguously demonstrating the successful introduction of quinoline into the pore of COF-366(Ni) structure (Figure 2b). The post-modification degree in this work is controlled to be almost similar by giving sufficient reaction time and a large excess of the aryl alkynes,[19] as also roughly evaluated by the peak disappearance of imine and the appearance of quinoline peaks in functionalized COFs in the FT-IR spectra at 1545 cm^{-1} and 1585 cm^{-1}, respectively (Figure 2b).[20] X-ray photoelectron spectroscopy demonstrates that the Ni sites in COF-366(Ni) and COF-366(Ni)-R are in the +2 oxidation state (Figure S1–S3).

The porosity and surface area of COF-366(Ni) and COF-366(Ni)-R have been examined by N_2 sorption isotherms at 77 K (Figure 2c). All the COFs displayed type-I adsorption/desorption isotherms, implying their microporous feature. The Brunauer–Emmett–Teller (BET) specific surface area of COF-366(Ni)-R is in the range of 136–644 m^2/g, which is smaller than the 960 m^2/g of COF-366(Ni). The decreased surface area is likely due to the occupation of the pores by the different-sized functional groups on the pore walls. Scanning electron microscopy (SEM) images of COF-366(Ni) and COF-366(Ni)-R illustrate irregular fibers-like morphology (Figure 2d, Figure S4–S5). Transmission electron microscope (TEM) images of COF-366(Ni)-CN and COF-366(Ni)-OMe show nanosheets with lattice fringes with a distance of 1.8 nm, which is corresponding to the (100) planes, further confirming the presence of highly ordered structures (Figure 2e).

In COF-366(Ni)-R, the periodic connections of porphyrin units and quinoline connections form porous π-conjugated scaffolds. Compared with the parent COF-366(Ni), the newly formed quinoline units through the Povarov reaction can enhance the π-conjugation of the resulting COFs to absorb light in the visible and near-infrared regions of the electromagnetic spectrum. Of greater significance, the diverse functional groups in the outer-sphere may further fine-tune the electronic properties of metals within the COFs. Therefore, COF-366(Ni) with different functional groups is expected to exhibit fascinating photoelectronic properties for photocatalytic oxidation of thioanisole.

To examine the photocatalytic performance of COF-366(Ni)-R, thioether oxidation, which is mediated by $^1O_2$,[5b,21] has been performed in CH_3CN under an O_2 environment with a violet light-emitting diode (LED light, 410–420 nm) (Figure 3a). As shown in Figure 3b, COF-366(Ni) gives a low yield of 12 % ± 1.24 % toward phenyl sulfoxide after 5 h. Interestingly, the reaction rates vary significantly for COF-366(Ni)-R depending on their -R functional groups. For example, the COF-366(Ni)-CN gives no observable yield under given reaction conditions. On the other hand, COF-366(Ni)-CF_3, which is functionalized with

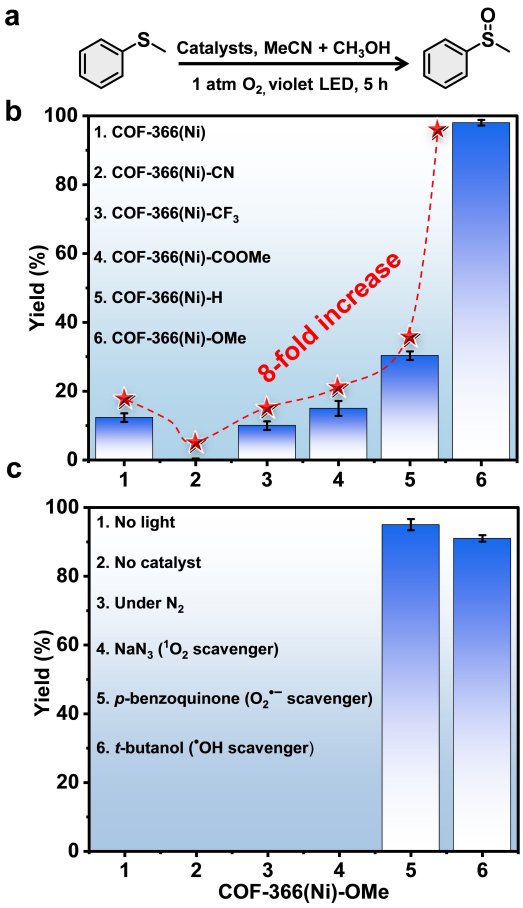

Figure 3. (a) Photocatalytic oxidation of thioether to phenyl sulfoxide. (b) The catalytic yield of the photocatalytic oxidation of thioether using COF-366(Ni) and COF-366(Ni)-R (the error bars in the graph indicate the relative standard deviation). (c) Yields of photocatalytic oxidation of thioether under different reaction conditions using COF-366(Ni)-OMe.

a weaker electron-withdrawing group than -CN, exhibits a low yield of 11 %. COF-366(Ni)-COOMe with a weak electron-withdrawing group displays a slightly higher yield of 17 %. Compared to the previous COFs, COF-366(Ni)-H demonstrates an improved yield of 30 %. In sharp contrast, a remarkable improvement in activity is observed in the presence of COF-366(Ni)-OMe with a strong electron-donating methoxyl group, which attains an exceptional yield of 98 %. The catalytic activity of COF-366(Ni)-R series for photocatalytic oxidative of thioether to sulfoxide follows the order of -CN < -CF_3 < -COOMe < -H < -OMe, which is in the same order as the electron-donating ability of the functional groups. In COF-366(Ni)-R series, the incorporation of different groups not only offers a significantly improved activity that can be up to 8-fold of the parent COF-366(Ni), but also achieves the switch of activity from nearly zero to 98 %. These results highlight the significant impact of different functional groups on the reactivity of porphyrin-based COFs in photocatalytic thioether oxidation.

Control experiments show that no product can be observed when the reaction is conducted without catalysts, in the dark, or in an N_2 atmosphere (Figure 3c), verifying

that the catalyst, light, and O_2 environment are indispensable for this oxidation reaction. The oxidation of thioether to phenyl sulfoxide is primarily mediated by $^1O_2$. Scavenging tests further confirm that $^1O_2$ is produced as the major ROS during the oxidation of thioanisole using COF-366(Ni)-OMe. As demonstrated in Figure 3c and Table S1, the reactions are completely inhibited by adding sodium azide (NaN_3) as the $^1O_2$ scavenger. In contrast, the introduction of $O_2^{\bullet-}$ scavenger (*p*-benzoquinone) and $^{\bullet}OH$ scavenger (*t*-butanol) has very limited influence on the yield.

It is worth noting that the functional groups influencing the light-assisted $^1O_2$ generation are not located in close proximity to the catalytic Ni(II) center. Instead, these functional groups should be assigned to the outer-sphere microenvironment of the Ni(II) center. It is generally believed that the metal center of porphyrin plays a vital role in the regulation of $^1O_2$ and, consequently, their catalytic activity.[15b] However, here, we have surprisingly demonstrated for the first time that the modulation of the outer-sphere microenvironment of catalytic metal sites could turn on and further tune the $^1O_2$ generation effectively.

Mechanistic study

To investigate the ability of COF-366(Ni) and COF-366(Ni)-R in the generation of ROS, including $^1O_2$ and $O_2^{\bullet-}$, we have conducted electron spin resonance (ESR) measurements on an aqueous suspension of the COF catalysts with the addition of $^1O_2$ and $O_2^{\bullet-}$ trapping agent, respectively. The 2,2,6,6-tetramethylpiperidine (TEMP) is utilized as a $^1O_2$ trapping agent, which generates the stable 2,2,6,6-tetramethylpiperidine oxide radical (TEMPO) upon capturing $^1O_2$. The 5,5-dimethyl-1-pyrroline-N-oxide (DMPO) is employed as $O_2^{\bullet-}$ trapping agent, which can be converted to DMPO-$O_2^{\bullet-}$ after capturing $O_2^{\bullet-}$. Strong and characteristic 1:1:1 triplet ESR signals of TEMPO are observed in the COF-366(Ni)-OMe system, demonstrating the $^1O_2$ production after light irradiation (Figure 4a, red curve).[5b] In contrast, no corresponding signals are observed in the COF-366(Ni)-CN systems (Figure 4b, purple curve). The relative signal intensities of TEMPO in the ESR spectra for the six COFs follow an order of COF-366(Ni)-CN < COF-366(Ni) < COF-366(Ni)-CF_3/COOMe < COF-366(Ni)-H < COF-366(Ni)-OMe, which is in a general consistence with the observed trend of the activity for these COFs. Interestingly, the relative signal intensities of DMPO-OOH (a spin adduct derived from DMPO-$O_2^{\bullet-}$) in the ESR spectra for the six COFs follow a reversed order as that of TEMPO (Figure 4b). These results clearly demonstrated that the excitonic behavior of COF-366(Ni)-R series is effectively modulated with the evolution of the functional groups from electron-withdrawing to electron-donating, resulting in weakened $O_2^{\bullet-}$ generation and enhanced $^1O_2$ generation.

It is generally believed that the production of $^1O_2$ relies on an energy transfer mechanism, specifically through the utilization of resonance energy transfer to excite O_2 molecules from their ground state via dipole-dipole interactions or charge exchange with photocatalyst.[22] In contrast to the energy transfer mechanism, the generation of $O_2^{\bullet-}$ involves an electron transfer mechanism, which involves the migration of charge carriers generated around active metal centers upon exposure to light towards the adsorbed O_2.[23] Therefore, at least three factors can be considered whether an energy or electron transfer process will occur between an excited semiconductor-based photocatalytic system and an O_2 molecule.[24] The first is the relative energy-level alignment between the photocatalyst and O_2. It will direct the flow of charge carriers between the O_2 and photocatalyst.[25] The second one is O_2 adsorption energy which will affect the likelihood of the electron transfer process. A strong O_2 adsorption energy favors the $O_2^{\bullet-}$ generation, whereas a weak O_2 adsorption promotes $^1O_2$ formation.[26] The third one is the composition of the frontier orbital of the photocatalyst. The π-type orbital shape favors overlapping with dioxygen's π frontier orbitals and enhances the likelihood of electron transfer to oxygen, favoring the $O_2^{\bullet-}$ generation. Conversely, the σ-type orbital has poor overlapping ability with dioxygen π frontier orbitals and hence limited electron transfer ability.[27]

To disclose the unique excitonic behavior of COFs in controlling the generation of $^1O_2$, we have first analyzed the electronic energy band levels of the COFs by performing light absorption measurements. All COFs exhibit a broad light absorption that extends to the near-infrared region, indicating their efficient light harvesting (Figure 4c). According to the calculations derived from the Tauc plots, the band gap energies are found quite close, which are 1.87, 1.72, 1.77, 1.70, 1.73, and 1.79 eV for COF-366(Ni), COF-366(Ni)-CN, COF-366(Ni)-CF_3, COF-366(Ni)-COOMe, COF-366(Ni)-H, and COF-366(Ni)-OMe, respectively (Figure S6–S11). We did not observe a significant difference in the band gaps of the post-modified COFs with different functional groups, which may be attributed to that the COFs share structural moieties, including nickel porphyrin and quinoline, and that the functional groups are not directly linked to those moieties. Interestingly, the valence band (VB) and conduction band (CB) levels of the COFs are distinct and are highly dependent on their functional groups (Figure 4d). As determined by Mott–Schottky plots (Figure S6–S11), the CB levels of COF-366(Ni), COF-366(Ni)-CN, COF-366(Ni)-CF_3, COF-366(Ni)-COOMe, COF-366(Ni)-H, and COF-366(Ni)-OMe are −0.55, −0.47, −0.51, −0.43, −0.53, and −0.15 V *vs* the normal hydrogen electrode (NHE, pH = 6.8). In COF-366(Ni)-R series, the CB energy levels become less negative when their -R group evolves from electron-withdrawing to electron-donating. Considering that the standard electrode potential for reduction of O_2 to $O_2^{\bullet-}$ ($E_0(O_2/O_2^{\bullet-})$ is −0.33 V,[28] the distinct CB levels in the COF-366(Ni)-R system could lead to different pathways for oxygen activation. COF-366(Ni)-R with strong electron-withdrawing groups (such as -CN and -CF_3) have CB levels much more negative than −0.33 V, which indicates that one-electron reduction of O_2 by the excited state of COF-366(Ni)-R with strong electron-withdrawing groups will be thermodynamically favorable.[29] In contrast, COF-366(Ni)-OMe with the least negative CB energy level of −0.15 V may not be able to initiate one-electron reduction of O_2 and

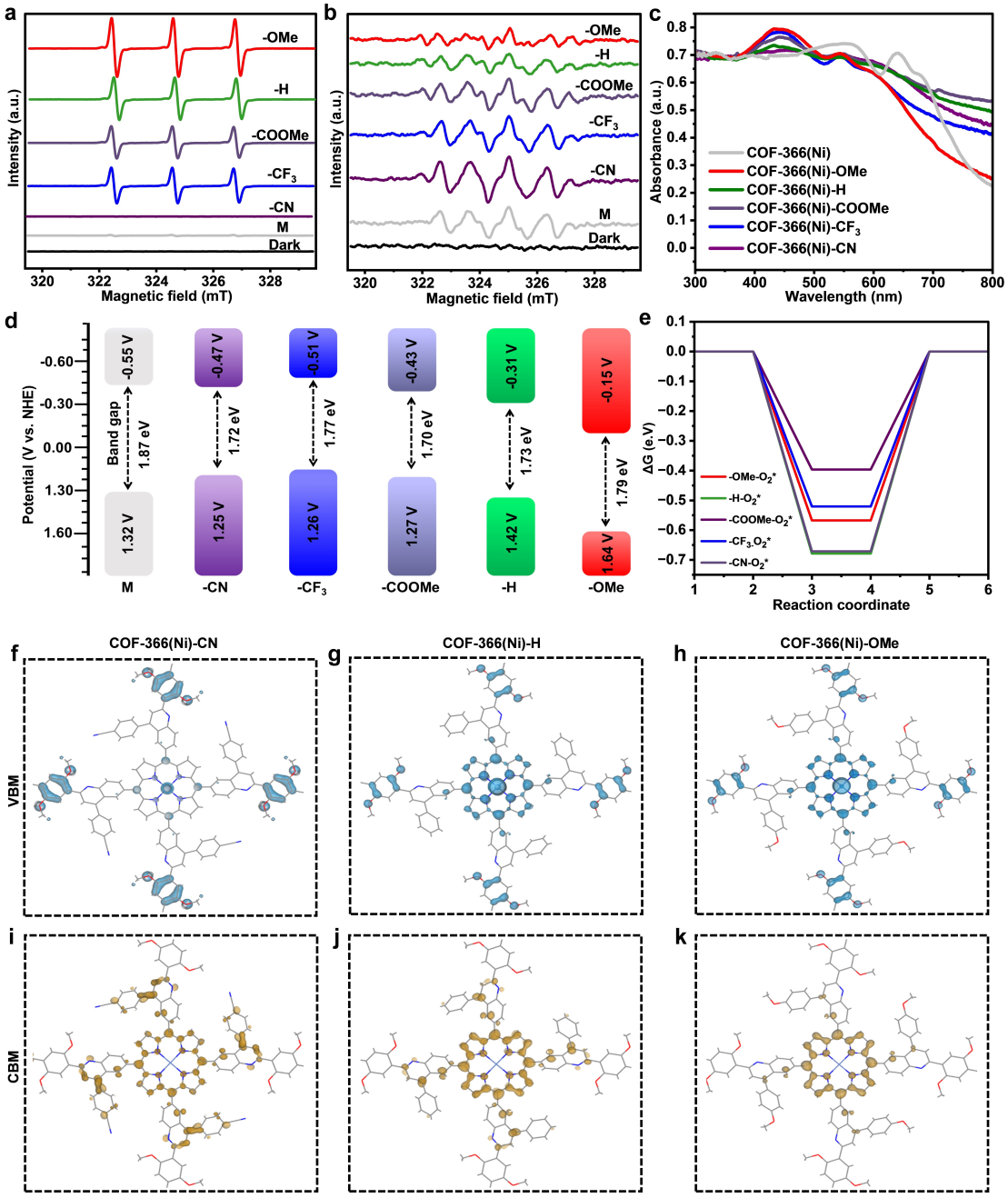

Figure 4. ESR spectra of COF-366(Ni) and COF-366(Ni)-R in the presence of (a) TEMP and (b) DMPO. (c) UV/Visible diffuse reflectance plots of COF-366(Ni) and COF-366(Ni)-R. (d) Band gaps of COF-366(Ni) and COF-366(Ni)-R. (e) Adsorption energies of O_2 on COF-366(Ni)-R. (f–h) VBM for COF-366(Ni)-CN, COF-366(Ni)-H, and COF-366(Ni)-OMe. (i–k) CBM for COF-366(Ni)-CN, COF-366(Ni)-H, and COF-366(Ni)-OMe. In (a), (b), and (d), M represents COF-366(Ni).

instead may promote the energy transfer process for the generation of $^1O_2$.

DFT calculations have been further conducted to get in-depth insights into the underlying mechanism of the distinct $^1O_2$ generation in the COF-366(Ni)-R series. As shown in Figure 4e, the calculated adsorption free energies (ΔG) between O_2 and different members of COF-366(Ni)-R series are quite close, which are all in the range of −0.40 to −0.68 eV. The absence of significant ΔG difference of O_2 adsorption for the COFs bearing electron-withdrawing or electron-donating groups can be rationalized by the fact that the O_2 adsorption is mainly determined by the electronic state of the Ni sites, which, however, can be hardly affected by the existence of the functional groups due to their spatial separation. Nevertheless, these results indicate that the binding strength of the COFs to O_2 is not a determinant factor that leads to distinct $^1O_2$ production in COF-366(Ni)-R series.

The frontier orbitals of COF-366(Ni)-R series have been further analyzed. As representative examples, COF-366(Ni)-

CN, COF-366(Ni)-H, and COF-366(Ni)-OMe bearing R groups from electron-withdrawing to electron-donating characteristics have been discussed in detail. Theoretical results show that the orbitals near the valency band maximum (VBM) for COF-366(Ni)-CN are mainly localized on the DMTA unit (Figure 4f), which show a prominent π-type characteristic. These π-type orbitals of COF-366(Ni)-CN are more likely to overlap with the π* frontier orbitals of O_2 due to the geometry match, facilitating the electron transfer from COF-366(Ni)-CN to O_2 upon excitation to form $O_2^{\bullet-}$. The orbitals near VBM of COF-366(Ni)-H are distributed on both porphyrin and DMTA units. Compared with those of COF-366(Ni)-CN, the VBM orbitals of COF-366(Ni)-H on DMTA units have weakened π feature and those distributed on the porphyrin ring show a prominent σ feature (Figure 4g), which may explain why COF-366(Ni)-H shows activity in the generation of both $O_2^{\bullet-}$ and $^1O_2$ in the ESR results. With the evolution of electron-donating characteristic of the -R group in COF-366(Ni)-OMe, VBM orbitals with more prominent σ feature are observed on both porphyrin and DMTA units (Figure 4h). On the contrary, orbitals near conduction band minimum (CBM) of COF-366(Ni)-CN, COF-366(Ni)-H, and COF-366(Ni)-OMe show opposite features with their orbitals near VBM, where the orbitals near CBM in COF-366(Ni)-OMe distributed on the porphyrin ring exhibit more pronounced π-type characteristic than those in COF-366(Ni)-H and COF-366(Ni)-CN (Figure 4i–k).

Through accessing the possible factors that affect the $^1O_2$ generation by experiments and theoretical calculations, the key factors that lead to the distinct $^1O_2$ generation capability in COF-366(Ni)-R series are mainly the energy level alignments and composition of their frontier orbitals. The outer-sphere microenvironment created by the functional groups with distinct electronic characteristics impacts these two factors as a function of their electron-withdrawing/-donating abilities, which successively result in the generations of $^1O_2$ in a trend of -CN < -CF_3 < -COOMe < -H < -OMe.

Conclusion

This study elucidated the impact of different functional groups surrounding catalytic nickel site based on a series of COFs containing electron-withdrawing and -donating groups on their pore walls. Notably, as the electronic property of functional groups evolves from electron-withdrawing to electron-donating, the adjusted outer-sphere surroundings trigger the photocatalytic performance, transforming it from almost zero product formation in the cyano group-functionalized COF to an outstanding 98 % yield achieved by the methoxy group-functionalized counterpart. Mechanistic study by electronic characterization and DFT calculations suggest that the distinct excitonic behaviors observed are linked to their band energy levels and orbital compositions of the COFs modulated by the outer-sphere microenvironment. Our study shows for the first time that, besides the generally used direct manipulation of catalytic metal sites, the modulation of the outer-sphere microenvironment around nickel site could turn on and further tune the $^1O_2$ generation effectively, which provides an essentially powerful strategy for improved catalytic performance.

Acknowledgements

This work was supported by the National Key Research and Development Program of China (2021YFA1500402), Strategic Priority Research Program of the CAS (XDB0450302), NSFC (22331009, U22A20401, 22161142001), the International Partnership Program of CAS (123GJHZ2022028MI) and the Scientific and Technological Research Council of Türkiye (TUBITAK, Grant No: 122N541).

Conflict of Interest

The authors declare no conflict of interest.

Data Availability Statement

The data that support the findings of this study are available from the corresponding author upon reasonable request.

Keywords: Covalent Organic Frameworks · Energy Transfer · Outer-Sphere Microenvironment · Photocatalysis · Singlet Oxygen

[1] L. Marzo, S. K. Pagire, O. Reiser, B. König, *Angew. Chem. Int. Ed.* **2018**, *57*, 10034–10072.
[2] a) T. J. Dougherty, C. J. Gomer, B. W. Henderson, G. Jori, D. Kessel, M. Korbelik, J. Moan, Q. Peng, *J. Natl. Cancer Inst.* **1998**, *90*, 889–905; b) A. P. Castano, T. N. Demidova, M. R. Hamblin, *Photodiagn. Photodyn. Ther.* **2004**, *1*, 279–293; c) X. Li, N. Kwon, T. Guo, Z. Liu, J. Yoon, *Angew. Chem. Int. Ed.* **2018**, *57*, 11522–11531.
[3] a) H. Wang, S. Chen, D. Yong, X. Zhang, S. Li, W. Shao, X. Sun, B. Pan, Y. Xie, *J. Am. Chem. Soc.* **2017**, *139*, 4737–4742; b) R. Long, K. Mao, X. Ye, W. Yan, Y. Huang, J. Wang, Y. Fu, X. Wang, X. Wu, Y. Xie, Y. Xiong, *J. Am. Chem. Soc.* **2013**, *135*, 3200–3207.
[4] R. D. Scurlock, B. Wang, P. R. Ogilby, J. R. Sheats, R. L. Clough, *J. Am. Chem. Soc.* **1995**, *117*, 10194–10202.
[5] a) Z. Ma, M. Zhang, X. Jia, J. Bai, Y. Ruan, C. Wang, X. Sun, X. Jiang, *Small* **2016**, *12*, 5477–5487; b) Y.-Z. Chen, Z. U. Wang, H. Wang, J. Lu, S.-H. Yu, H.-L. Jiang, *J. Am. Chem. Soc.* **2017**, *139*, 2035–2044; c) D. Wang, X. Wang, S. Zhou, P. Gu, X. Zhu, C. Wang, Q. Zhang, *Coord. Chem. Rev.* **2023**, *482*, 215074; d) C. Li, J. Liu, Y. Hong, R. Lin, Z. Liu, M. Chen, J. W. Y. Lam, G.-H. Ning, X. Zheng, A. Qin, B. Z. Tang, *Angew. Chem. Int. Ed.* **2022**, *61*, e202202005; e) J. Zhao, W. Wu, J. Sun, S. Guo, *Chem. Soc. Rev.* **2013**, *42*, 5323–5351.
[6] H. Wang, S. Jiang, S. Chen, D. Li, X. Zhang, W. Shao, X. Sun, J. Xie, Z. Zhao, Q. Zhang, Y. Tian, Y. Xie, *Adv. Mater.* **2016**, *28*, 6940–6945.
[7] a) W. C. Howland, J. B. Gerken, S. S. Stahl, Y. Surendranath, *J. Am. Chem. Soc.* **2022**, *144*, 11253–11262; b) W. Wu, Q. Zhang, X. Wang, C. Han, X. Shao, Y. Wang, J. Liu, Z. Li, X. Lu, M. Wu, *ACS Catal.* **2017**, *7*, 7267–7273.

[8] a) J. M. Dąbrowski, B. Pucelik, A. Regiel-Futyra, M. Brindell, O. Mazuryk, A. Kyzioł, G. Stochel, W. Macyk, L. G. Arnaut, *Coord. Chem. Rev.* **2016**, *325*, 67–101; b) X. Zhan, D. Kim, Z. Ullah, W. Lee, Z. Gross, D. G. Churchill, *Coord. Chem. Rev.* **2023**, *495*, 215363.
[9] L. Jiao, J. Wang, H.-L. Jiang, *Acc. Mater. Res.* **2021**, *2*, 327–339.
[10] a) Y. Meng, Y. Luo, J.-L. Shi, H. Ding, X. Lang, W. Chen, A. Zheng, J. Sun, C. Wang, *Angew. Chem. Int. Ed.* **2020**, *59*, 3624–3629; b) R. Chen, J.-L. Shi, Y. Ma, G. Lin, X. Lang, C. Wang, *Angew. Chem. Int. Ed.* **2019**, *58*, 6430–6434; c) Q.-Y. Wang, J. Liu, M. Cao, J.-H. Hu, R. Pang, S. Wang, M. Asad, Y.-L. Wei, S.-Q. Zang, *Angew. Chem. Int. Ed.* **2022**, *61*, e202207130.
[11] a) S. A. Cook, A. S. Borovik, *Acc. Chem. Res.* **2015**, *48*, 2407–2414; b) M. Raynal, P. Ballester, A. Vidal-Ferran, P. W. N. M. van Leeuwen, *Chem. Soc. Rev.* **2014**, *43*, 1734–1787.
[12] a) A. J. Neel, M. J. Hilton, M. S. Sigman, F. D. Toste, *Nature* **2017**, *543*, 637–646; b) F. D. Toste, M. S. Sigman, S. J. Miller, *Acc. Chem. Res.* **2017**, *50*, 609–615; c) L. Liu, T.-Y. Zhou, S. G. Telfer, *J. Am. Chem. Soc.* **2017**, *139*, 13936–13943; d) M. Zhao, K. Yuan, Y. Wang, G. Li, J. Guo, L. Gu, W. Hu, H. Zhao, Z. Tang, *Nature* **2016**, *539*, 76–80.
[13] a) J. Meeuwissen, J. N. H. Reek, *Nat. Chem.* **2010**, *2*, 615–621; b) N. A. Grosso-Giordano, C. Schroeder, A. Okrut, A. Solovyov, C. Schöttle, W. Chassé, N. Marinković, H. Koller, S. I. Zones, A. Katz, *J. Am. Chem. Soc.* **2018**, *140*, 4956–4960.
[14] a) A. P. Cote, A. I. Benin, N. W. Ockwig, M. O′Keeffe, A. J. Matzger, O. M. Yaghi, *Science* **2005**, *310*, 1166–1170; b) K. Geng, T. He, R. Liu, S. Dalapati, K. T. Tan, Z. Li, S. Tao, Y. Gong, Q. Jiang, D. Jiang, *Chem. Rev.* **2020**, *120*, 8814–8933; c) D. W. Burke, R. R. Dasari, V. K. Sangwan, A. K. Oanta, Z. Hirani, C. E. Pelkowski, Y. Tang, R. Li, D. C. Ralph, M. C. Hersam, *J. Am. Chem. Soc.* **2023**, *145*, 11969–11977; d) H. Li, A. Dilipkumar, S. Abubakar, D. Zhao, *Chem. Soc. Rev.* **2023**, *52*, 6294–6329; e) S. Yang, W. Hu, X. Zhang, P. He, B. Pattengale, C. Liu, M. Cendejas, I. Hermes, X. Zhang, J. Zhang, J. Huang, *J. Am. Chem. Soc.* **2018**, *140*, 14614–14618; f) S. Zhang, G. Cheng, L. Guo, N. Wang, B. Tan, S. Jin, *Angew. Chem. Int. Ed.* **2020**, *59*, 6007–6014; g) Q. Fang, S. Ma, *Macromol. Rapid Commun.* **2023**, *44*, 2300203; h) Y. Yang, X. Chu, H.-Y. Zhang, R. Zhang, Y.-H. Liu, F.-M. Zhang, M. Lu, Z.-D. Yang, Y.-Q. Lan, *Nat. Commun.* **2023**, *14*, 593.
[15] a) X.-R. Ren, B. Bai, Q. Zhang, Q. Hao, Y. Guo, L.-J. Wan, D. Wang, *J. Am. Chem. Soc.* **2022**, *144*, 2488–2494; b) Y. Qian, D. Li, Y. Han, H.-L. Jiang, *J. Am. Chem. Soc.* **2020**, *142*, 20763–20771.
[16] A. Volkov, J. Mi, K. Lalit, P. Chatterjee, D. Jing, S. L. Carnahan, Y. Chen, S. Sun, A. J. Rossini, W. Huang, L. M. Stanley, *J. Am. Chem. Soc.* **2023**, *145*, 6230–6239.
[17] C. S. Diercks, S. Lin, N. Kornienko, E. A. Kapustin, E. M. Nichols, C. Zhu, Y. Zhao, C. J. Chang, O. M. Yaghi, *J. Am. Chem. Soc.* **2018**, *140*, 1116–1122.
[18] X. Li, C. Zhang, S. Cai, X. Lei, V. Altoe, F. Hong, J. J. Urban, J. Ciston, E. M. Chan, Y. Liu, *Nat. Commun.* **2018**, *9*, 2998.
[19] a) V. V. Kouznetsov, *Tetrahedron* **2009**, *65*, 2721–2750; b) O. Ghashghaei, C. Masdeu, C. Alonso, F. Palacios, R. Lavilla, *Drug Discovery Today Technol.* **2018**, *29*, 71–79.
[20] a) X.-T. Li, J. Zou, T.-H. Wang, H.-C. Ma, G.-J. Chen, Y.-B. Dong, *J. Am. Chem. Soc.* **2020**, *142*, 6521–6526; b) N. Shindoh, H. Tokuyama, Y. Takemoto, K. Takasu, *J. Org. Chem.* **2008**, *73*, 7451–7456.
[21] S. Jin, W. Shao, X. Luo, H. Wang, X. Sun, X. He, X. Zhang, Y. Xie, *Adv. Mater.* **2022**, *34*, 2206516.
[22] a) L. Cao, Z. Lin, W. Shi, Z. Wang, C. Zhang, X. Hu, C. Wang, W. Lin, *J. Am. Chem. Soc.* **2017**, *139*, 7020–7029; b) R. Haldar, M. Jakoby, A. Mazel, Q. Zhang, A. Welle, T. Mohamed, P. Krolla, W. Wenzel, S. Diring, F. Odobel, B. S. Richards, I. A. Howard, C. Wöll, *Nat. Commun.* **2018**, *9*, 4332.
[23] H. Wang, X. Sun, D. Li, X. Zhang, S. Chen, W. Shao, Y. Tian, Y. Xie, *J. Am. Chem. Soc.* **2017**, *139*, 2468–2473.
[24] J. T. DuBose, P. V. Kamat, *Chem. Rev.* **2022**, *122*, 12475–12494.
[25] Z. Zhu, H. Huang, L. Liu, F. Chen, N. Tian, Y. Zhang, H. Yu, *Angew. Chem. Int. Ed.* **2022**, *61*, e202203519.
[26] M. A. Henderson, W. S. Epling, C. L. Perkins, C. H. F. Peden, U. Diebold, *J. Phys. Chem. B* **1999**, *103*, 5328–5337.
[27] Y.-Q. Zou, J.-R. Chen, X.-P. Liu, L.-Q. Lu, R. L. Davis, K. A. Jørgensen, W.-J. Xiao, *Angew. Chem. Int. Ed.* **2012**, *51*, 784–788.
[28] H. Tan, P. Zhou, M. Liu, Q. Zhang, F. Liu, H. Guo, Y. Zhou, Y. Chen, L. Zeng, L. Gu, Z. Zheng, M. Tong, S. Guo, *Nat. Synth.* **2023**, *2*, 557–563.
[29] C. Yu, J. He, M. Tan, Y. Hou, H. Zeng, C. Liu, H. Meng, Y. Su, L. Qiao, T. Lookman, Y. Bai, *Adv. Funct. Mater.* **2022**, *32*, 2209365.

Manuscript received: October 6, 2023
Accepted manuscript online: November 28, 2023
Version of record online: December 8, 2023